Journal of Building Engineering 98 (2024) 111441

Contents lists available at ScienceDirect

Journal of Building Engineering

journal homepage: www.elsevier.com/locate/jobe

Recycled ceramic brick powder utilization in fiber reinforced 3D printing concrete: An eco-friendly substitute to conventional fine aggregates

Bo Huang [a], Yutian Ge [a], Xiangyu Wang [b], Yufei Wang [c], Jianqun Wang [a], Chengwei Song [d], Jun Zhu [b], Chiemela Victor Amaechi [e], Junbo Sun [f,*]

[a] School of Civil Engineering, Hunan University of Science and Technology, Xiangtan, 411201, China
[b] School of Civil Engineering and Architecture, East China Jiao Tong University, Nanchang, 330013, China
[c] School of Design and the Built Environment, Curtin University, Perth, WA 6102, Australia
[d] Jiangsu Langqi High-Tech Technology Co., Ltd, Lianyungang, 222000, China
[e] Engineering Department, Lancaster University, Gillow Avenue, Bailrigg, Lancaster, LA1 4YW, UK
[f] Chongqing University, Chongqing, 400044, China

ARTICLE INFO

Keywords:
3D printing
Recycled ceramic brick powder
Mechanical properties
SEM
Porosity
Environmental impact

ABSTRACT

The incorporation of recycled ceramic brick powder (RCBP) into conventional cast concrete has proofed its efficacy in substituting aggregates, improving strength, and contributing to environmental sustainability. Concurrently, 3D printing technology is emerging as a pivotal trend in intelligent construction. This study investigates the collaborative interaction mechanisms of 3D-printed RCBP concrete. Compressive and four-point bending tests along the x, y, and z-axis are conducted to evaluate its strength and anisotropy. Subsequently, the hydration products and pore structural characteristics were analyzed employing Scanning Electron Microscope (SEM) and X-CT experiments. Additionally, an environmental life cycle analysis is performed utilizing OpenLCA software. The results determined an optimal RCBP content of 25-wt% yields satisfactory performance in macro-mechanical properties (with maximal 65.57 MPa for compressive strength and 12.66 MPa for flexural strength) and micro-structural characterization. Specifically, the drainage consolidation effect achieved through 3D printing technology mitigates the typical decline observed in conventional RCBP concrete. However, exceeding the 25-wt% threshold leads to a noticeable decline in mechanical strength due to inhomogeneous particle gradation and excessive aggregation of RCBP particles, despite a significant reduction in porosity. Furthermore, as RCBP incorporation increases from 0-wt% to 100-wt%, four environment impact indicators including Global warming potential (GWP), Acidification Potential (AP), Ozone Depletion Potential (ODP), and Abiotic depletion potential (ADP) respectively decline by 24.86 %, 6.59 %, 0.49 %, and 0.62 %, demonstrating exceptional environmental benefits. Notably, the tremendous influence on GWP is attributed to the remarkable carbon sequestration of RCBP, aligning with national carbon neutrality goals and advancing sustainable construction practices.

* Corresponding author.
E-mail addresses: bohuang@hnust.edu.cn (B. Huang), 3244722548@qq.com (Y. Ge), 604698492@qq.com (X. Wang), wangyf0113_suz@163.com (Y. Wang), jqw@hnust.edu.cn (J. Wang), 173755025@qq.com (C. Song), zj1817970@163.com (J. Zhu), Chiemelavic@gmail.com (C.V. Amaechi), tunneltc@gmail.com (J. Sun).

https://doi.org/10.1016/j.jobe.2024.111441
Received 5 September 2024; Received in revised form 19 November 2024; Accepted 27 November 2024
Available online 29 November 2024

1. Introduction

Rapid urbanization and industrialization contribute to the increased solid waste generation, which is estimated to increase by 3.88 billion tons in 2050 [1]. Besides, the civil engineering construction process continuously releases carbon dioxide, sulfur dioxide, and other oxides, driving global warming and other environmental issues toward more pessimistic outcomes [2–5]. Although waste materials reuse action has been implemented worldwide, large amounts of landfill waste still face challenges to be resolved. Especially, construction and demolition (C&D) waste occupies the majority of landfill and solid waste and generates around 3 billion tons per year [6]. The C&D waste is mostly composed of concrete [7], bricks [8], and rocks [9], but only 30 % of C&D waste can be recycled through diverse methods, while the other 60 % is extremely tough to recover and finally discarded in landfills [6]. Recycled ceramic brick powder (RCBP) serves as the major recycled component of brick waste, occupying an abundant percentage of C&D waste. Nevertheless, ceramic brick waste suffers minimal recovery efficiency and narrowly direct usage scenarios, restricting its widespread application. Therefore, there is an imperative to investigate novel recycling methodologies to transform RCBP into available resources, thereby effectively mitigating oxide emissions.

RCBP concrete usually yields outstanding mechanical performance, thermal expansion reliance, and stability that are massively attributed to the high-temperature resistant and durable ceramic powder [10]. For instance, Tang et al. [11] discovered that 30 % RBP-incorporated concrete enabled the pore ratio below 10 nm to increase by 30 % at 28 days, massively reinforcing the porous composition. Dang et al. [12] investigated that $Ca(OH)_2$ inclusion in concrete is remarkably reduced by 56 %–58 % when recycled brick (RB) replaced 100 % sand aggregate, which is attributed to the pozzolanic reactivity of RB. Sahoo et al. [13] revealed that the combination of RBP materials and carbon sequestration implemented in concrete significantly decreases carbon inclusion, promoting carbon sequestration around 30–82 %. Shrivastava et al. [14] confirmed that 5 % RBP addition massively enhances concrete compressive strengths by 11.6 % at 28 days. In conclusion, RCBP applied in enormous studies demonstrated its outstanding potential to facilitate the mechanical performance of concrete, indirectly assisting in mitigating the burden on C&D waste and resource shortage. However, the traditional casting production process suffers from a deficiency in formwork materials waste [15] and inflexible manufacture [16], thus novel generation technologies are eagerly anticipated to be utilized in RCBP concrete.

3D concrete printing (3DCP), based on digital and automatic technology, builds 3D structures through layer-by-layer accumulation process. This technology has acquired worldwide attention for its inherent merits, including fewer workforce requirements [17], increasing manufacturing productivity [18], and simplified construction process [19]. Besides, the 3D printing crafts, printable materials, and environmental efficiency in the construction industry have been widely probed by researchers [20,21]. Xiao et al. [22] compared the large-scale 3DCP with laboratory 3DCP and presented that printing geometrically simple shapes has been demonstrated to be cost-effective and efficient compared to traditional construction methods. Muñoz et al. [23] verified that the-3D-printing is an environmentally friendly construction method, decreasing GHG emission by 38 % compared to disposable building structures. Recently, recycled solid waste (RSW) has provided a new perspective for 3D printable composites and considerable studies have also been conducted on the characteristics of RSW [24,25]. Ding et al. [26] produced 3DCP by incorporating recycled sand (RS) and discovered that tensile and flexural properties respectively reach a maximum of 2.8 MPa and 4.5 MPa with 50 % embodied RS. Ma et al. [27] introduced copper tailings aggregates (CTA) to 3D mixes and confirmed that a 30 % addition of CTA achieves excellent flowability and strength. Liu et al. [28] claimed that recycled glass (RG) as sand replacement within 3D-printing concrete improves flexural ability by 25 %–30 %. Accordingly, the cooperation of RCBP and 3D printing concrete unveils promising prospects for innovation in 3D-printed construction engineering.

Nevertheless, the macroscopic properties of 3DCP incorporating waste materials as substitutes are inferior to concrete manufactured by original materials. Consequently, various fiber applications exhibit the potential to enhance the anisotropy and compensate for the strength deficiencies of 3D-printed solid waste concrete, ascribing to its distinctive benefits of improving materials' microstructure and toughness and controlling crack propagation. Singh et al. [29] found that a 75 % antimony tailings (AT) ratio in fiber-enhanced 3D printed mix achieves excellent printable capability and the highest strength up to 105 MPa, and presents excellent strength in x-direction. Yang et al. [30] proposed that 20 % RBCP utilized to replace cement in PP fiber-enhanced 3DCP realized 55.9 MPa for compressive strength and 12.49 MPa for flexural strength. Meanwhile, remarkable thermal reliance at 300 °C was observed and an anisotropic regulation adhered to $F_x < F_y < F_z$ was determined. Sun et al. [31] applied PVA fiber in three-dimensional lightweight engineered cementitious composites (LWECCs), whose unconfined compression strength and flexural strength respectively reached excellent 33.6 MPa and 9.29 MPa in the z-axis. Concurrently, few studies have focused on the mechanical behavior of 3DCP with combined RCBP aggregates, PP fiber, and antimony tailing. This research is driven by the necessity to confront two critical global challenges: the escalating accumulation of C&D waste and the environmental repercussions of traditional construction methodologies. Notably, the recycling of ceramic brick waste presents substantial promise as a solution, yet it remains a relatively underinvestigated domain, particularly within the framework of 3DCP. Nevertheless, the compatibility and applicability between RCBP and 3DCP still require further analysis and exploration.

This study investigated the synergistic impact mechanisms of RCBP to replace grit in fiber-reinforced 3D printing concrete. 62 test blocks at five varying replacement rates (0-wt%, 25-wt%, 50-wt%, 75-wt%, 100-wt%) of RCBP were applicated throughout the entire process. The early-stage properties, particularly the buildability and rheology comprising yield stress and viscosity of RCBP-3DCP were initially examined and measured. Subsequently, five groups of samples are prepared for compressive and flexural tests and each group has three identical samples, whilst the other 47 specimens are utilized for microstructure inspection. The objective is to confirm the optimal hardened performances, evaluate the anisotropy along the x, y, and z-axes, and determine the internal structure in 3D printing RCBP mixtures. Furthermore, a scanning electron microscope (SEM) was adopted to analyze the cement paste-aggregate interface and

interlayer bonding area. Besides, advanced Computed Tomography (CT) was utilized to explore the porosity and spatial layout inside the pre-experiment samples. Eventually, four indicators proposed by the CML (Centrum voor Milieukunde Leiden) life cycle assessment methodology were chosen for a comprehensive environmental impact evaluation of a 3D-printed RCBP mixture. This study provides novel insights into the sustainable evolution of 3D-printed concrete, elucidating how the integration of waste materials, such as RCBP, not only mitigates the carbon footprint but also fosters resource recycling, thereby catalyzing the shift towards a circular economy in the construction sector.

2. Methodology

2.1. Materials

The experiment utilized Ordinary Portland cement (OPC 42.5) and silica fume (SF) of grade 955 as cementitious materials. Coarse sand in the size range of 0.075–4.750 mm and fine sand in the sand range of 0.075–2.36 mm were prepared. Recycled brick powder (RCBP) is extracted from waste bricks to replace coarse sand as an eco-friendly alternative, ranging from 0.75 mm to 1.25 mm. The granulometric distribution of coarse sand, RCBP, and fine sand are demonstrated in Fig. 1. Antimony tailings (AT) and polypropylene (PP) fibers with a length of 6 mm were incorporated to compensate for the flexural property and reduce cracks due to the absence of reinforcement. The morphologies of OPC, SF, RP, and PP fiber are shown in Fig. 2.

The mix volume proportions of RCBP adopted at five designs (0-wt%, 25-wt%, 50-wt%, 75-wt%, 100-wt%) are listed in Table 1. Most studies focus on RCBP replacement ratios of 0%–30 % [32–35], while our study uses a broader range of 0∼100-wt% to provide a more comprehensive evaluation. Compared to steel and carbon fibers, PP fibers are more affordable and do not affect the flowability or printability of 3D printed concrete. Consequently, we determined the design parameters for RCBP content and the type of fibers through orthogonal experiments.

The chemical constituents of SF, OPC, and AT are presented in Table 2, while the physical performances of PP fiber are demonstrated in Table 3. Moreover, additives including hydroxypropyl methylcellulose (HPMC) with a viscosity of 200000 mPa s, nano clay (NC), sodium gluconate (SG), and polycarboxylate-based superplasticizer (SP) are introduced to enable the fresh concrete to acquire outstanding thixotropy, buildability, flowability and achieve flexible control on the setting time of mortar. Additionally, Elastic modulus and softness matrix of various RCBP concrete are shown in Table 4.

2.2. Sample preparation

Primarily, all dry ingredients except HPMC, PP fibers, and NC, were integrated using a 60 L horizontal mixing machine for 120 s at a lab temperature of about 23 ± 1 °C, followed by adding water to the mixer container for 3 min. Afterward, the HMPC and powdered NC were introduced until the mix possessed appropriate uniformity and flowability for 1 min. Furthermore, the PP fibers were incorporated at a slow pace to attain a homogeneous fiber dispersion, and mixed for additional 180 s. Thereafter, the above-mixed materials were placed into the printer hopper and printed based on a prepared digital model. Subsequently, the printed samples were insulated from the external environment with plastic film to promote hydration on the printing platform and demolded after 24 h. Finally, all specimens were cured at a relative moisture of 40 ± 5 % and an ambient temperature of 23 ± 1 °C before the mechanical tests at 14 d and 28 d.

A gantry-style 3D concrete printing machine is employed to produce RCBP-incorporated concrete, with a printing range of 1.6 m × 1.5 m × 1.5 m as represented in Fig. 3. The major devices consist of the control system, 3 moving sliders, a printhead, and an automatic hopper. Moreover, the printhead is composed of a worm stirring screw and a round print nozzle with a diameter of 15 mm. Besides, a worm pump enables fresh mix to be transferred into the printer hopper at a consistent rate. After that, a fresh concrete filament with 15 mm in breadth and 6 mm in height was extruded stably from the nozzle according to a pre-designed route. Additionally, the pumping and extrusion velocities were respectively kept at 50 mm/s and 8830 mm^3/s. Meanwhile, the print head was continuously moving in the X, Y, and Z sliders to formulate 3D layer-by-layer structures.

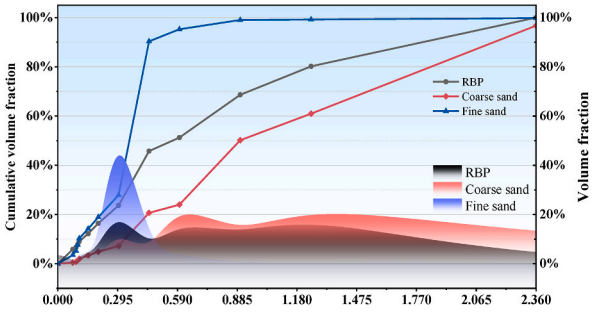

Fig. 1. The particle size distribution of coarse sand, RCBP, and fine sand.

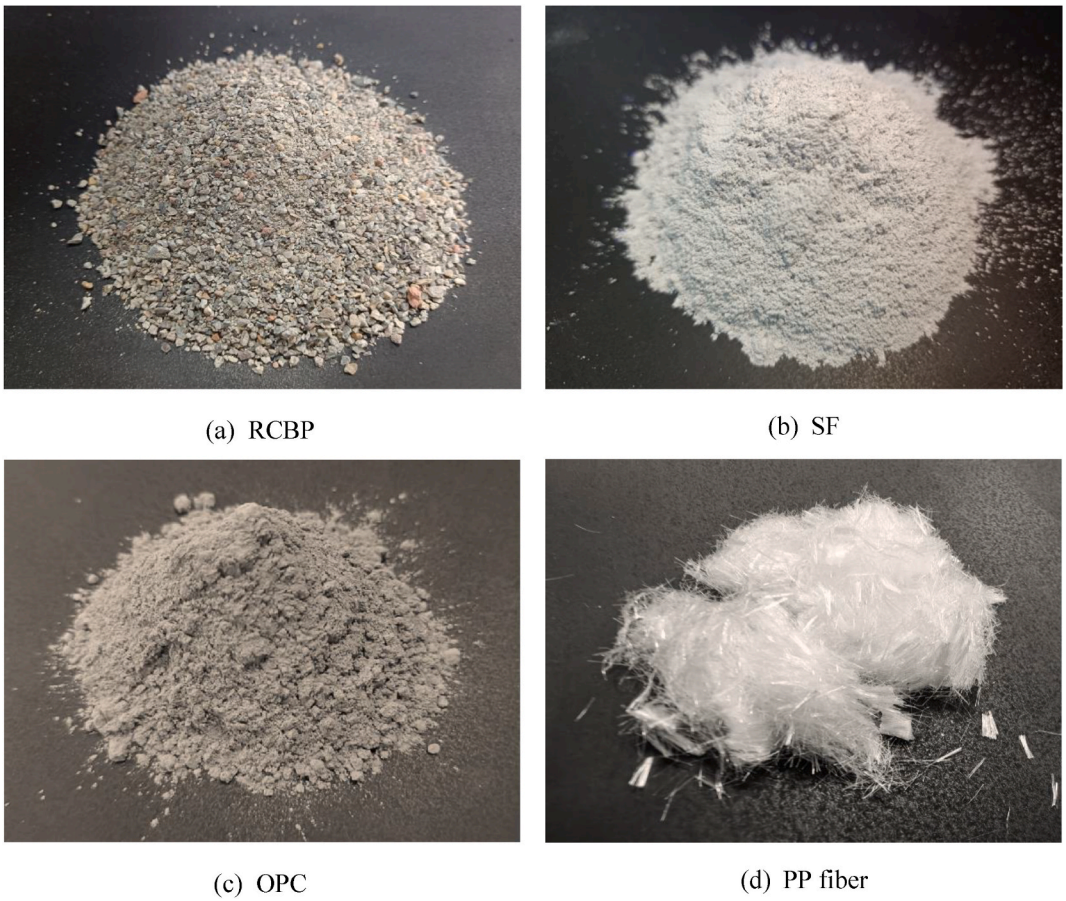

Fig. 2. Morphologies of RCBP, SF, OPC, and PP fiber.

Table 1
Mixture design for the printable samples (g).

Symbol	Cement	SF	Coarse Sand	RC BP	Fine sand	AT	PP fiber	Deformer	HPMC	SP	NC	SG	Water
Control	1200	120	300	0	172.5	517.5	2	1	4	4	3	1	405
RCBP-25	1200	120	225	75	172.5	517.5	2	1	4	4	3	1	405
RCBP-50	1200	120	150	150	172.5	517.5	2	1	4	4	3	1	405
RCBP-75	1200	120	75	225	172.5	517.5	2	1	4	4	3	1	405
RCBP-100	1200	120	0	300	172.5	517.5	2	1	4	4	3	1	405

Table 2
Chemical constituents of OPC, SF, and AT (wt%).

Material	SiO_2	Fe_2O_3	MgO	CaO	Al_2O_3	SO_3	Na_2O	P_2O_5	SO_3	ZnO	MnO	TiO_2	FeO
OPC	20.10	2.80	1.30	63.4	4.60	2.70	0.60	–	2.70	–	–	–	–
SF	98.32	0.13	0.14	0.15	0.38	0.68	–	0.07	0.68	0.05	–	–	–
AT	88.8	0.98	0.11	0.61	3.86	–	0.02	0.04	–	–	0.03	0.30	0.27

Table 3
Mechanical and physical performances of PP fiber.

Fiber	Density ρ (g/cm^3)	Tensile strength $f_{t\,f}$ (MPa)	Elastic modulusE_f (GPa)	Rupture elongation (%)	Length L_f (mm)	Average Diameter d_f (μm)	Aspect ratio L_f/d_f
PP	0.91	460	3.5	30	6	31	193.5

Table 4
Elastic modulus and softness matrix of various RCBP concrete.

Property	Control	RCBP-25	RCBP-50	RCBP-75	RCBP-100
Elastic modulus (GPa)	21.6	22.3	20.4	18.9	17.1
Softness matrix (Pa^{-1})	4.63×10^{-11}	4.48×10^{-11}	4.90×10^{-11}	5.29×10^{-11}	5.85×10^{-11}

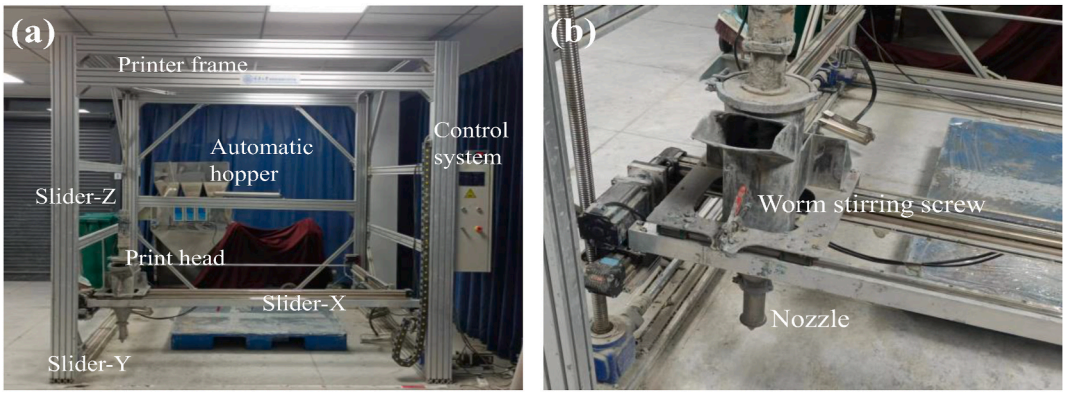

Fig. 3. The general frame of (a) the 3D printer equipment and (b) the detailed printhead structure.

2.3. Experimental methods

2.3.1. Buildability

Buildability refers to the geometric stabilization capacity to construct multi-layer structures with adequate moldability and favorable deformation resistance. Meanwhile, buildability is considered a crucial parament to exhibit variable rheology performance, especially plasticity viscosity and dynamic/static shear stress. Li et al. [36] investigated quantitative evaluation for buildability in equation (1):

$$\triangle h = \frac{H - H'}{H} \times 100\% \tag{1}$$

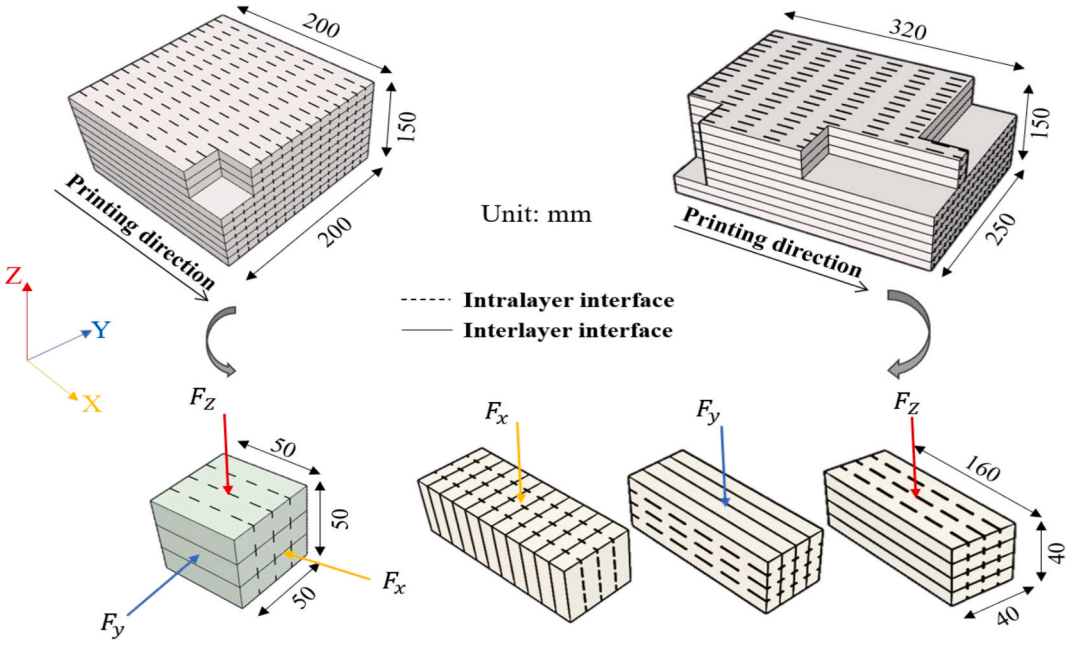

Fig. 4. Samples subject to anisotropic loading directions and compressive and flexural experiment.

Where $\triangle h$ represents the cumulative deformation rate of the printed wall height, H refers to the theoretical height of the printed wall (i.e. the nozzle height of the 3D printer), H' is the actual height of the printed wall.

As reported in their findings, when $\triangle h$ does not exceed 6 %, the dynamic yield stress ranges from 200 to 800 Pa, and the static yield stress varies between 1800 and 3300 Pa, the mortar exhibits a remarkable capacity for achieving a high number of printable layers (higher than 30), thereby ensuring superior buildability. The standability test was implemented to measure the stack height to assess the buildability of RCBP 3DCP, which printed concrete into designed shapes in this experiment.

2.3.2. Mechanical strength

The compression and flexural capacities of trial specimens with all various mix-ratio designs were measured by an automatic pressure tester conforming to GB/T 50081-2019 [37] and GB/T 17671-2021 [38]. Furthermore, all specimens were obtained from 3DCP slabs at 28d and three identical test blocks were ready for each diverse design ratio. Afterward, these samples experienced load in 3 vertical directions to symbolize the anisotropy of RCBP concrete, which is illustrated in Fig. 4. The x-axis maintains parallelism with the printing direction, the y-axis keeps orthogonal to the intralayer interface, and the z-axis remains perpendicular to the printing trajectory and interlayer interface. Furthermore, the loading rates of compressive and flexural tests are respectively designed to 0.5–0.8 MPa/s and 0.5 mm/min. Both experiments will consider the average of the three sample measurements as the final result at 28 days to reduce production and inspection errors.

In addition, the compressive behavior f_c is quantified by the following equation employing cube samples with a size of 50 × 50 × 50 mm^3:

$$f_c = \frac{F_c}{A_c} \tag{2}$$

Where F_c symbols the maximum loading value, while A_c means the area under pressure.

The flexural ability was derived from a three-point bending experiment and calculated through the following formula utilizing rectangular samples with a dimension of 40 × 40 × 160 mm^3:

$$f_f = \frac{3F_f L}{2bh^2} \tag{3}$$

Where F_f is maximum bending strength, L represents the span, and the width and height of the sample are respectively denoted by b and d.

2.3.3. Microstructure analysis

Scanning electron microscope (SEM) and X-ray computed tomography (X-CT) tests are extensively applicated to identify the microstructures of construction materials. SEM was conducted by Quanta FEG in the secondary electron pattern with the operating voltage of 10 kV and magnification ranging from 100×, 200x, 500x, 1000x, 5000x, 10000x to 30000x. The X-CT with a density resolution of 1 %, a spatial resolution of 2.8 LP/mm, and a peak penetration capacity of over 60 mm steel was adopted. Meanwhile, The CT scanner employed achieves high-precision observation of concrete pore structure (i.e. pore size dispersion, porosity) and holds a scanning range of 310 mm × 600 mm. Besides, the machine is equipped with a digital flat-panel x-ray detector and a 450 KV small focused radiation source.

2.3.4. Environmental evaluation

The environmental impact evaluation in this investigation adhered to ISO 14040 [39] and employed OpenLCA software.

(i) Goal and scope definition: 1 m^3 3D-printed concrete with cement, SF, AT, PP-fiber, and RCP (as shown in Table 1) is recognized as the functional unit. Besides, the system perimeter encompasses extracting raw materials essential for fabricating the mixture, as well as the concrete manufacturing process implemented in the experimental lab.

(ii) Life cycle inventory analysis: The OpenLCA software, which is perfectly compatible with the terminology and outline of ISO 14040, is utilized to generate inventory flows for modeling. Inventory flows in this paper comprise inputs of the primary components applied in RCBP 3DCP (i.e. cement, SF, coarse sand, RCBP, fine sand, AT, PP fiber, and water), alongside the outputs from concrete formulation and emissions to water, land, and air. These inventory flows are derived from the Ecoinvent v3.8 information database.

(iii) Life cycle impact assessment: Global warming potential (GWP), Acidification Potential (AP), Ozone Depletion Potential (ODP), and Abiotic depletion potential (ADP) are selected as environmental outcomes indicators. CML, an environment impact assessment method specified in EN15804 [40], is applicated to analyze the environmental implications of the blending procedure to manufacture 1 m^3 concrete as well as depict and standardize the environmental consequences index. Four indicators present the characterization results in actual units: GWP is measured in kg carbon dioxide (CO_2) equivalent, AP is assessed in kg sulfur dioxide (SO_2) equivalent, ODP is quantified in kg chlorofluorocarbon-11 (CFC-11) equivalent, and ADP is evaluated in kg antimony equivalent. Meanwhile, these indicators are regulated by multiplying the characterized results by the reciprocal of the overall equivalent discharges in that influence category annually affiliated with a complete geographic zone [41]. The standardization database (a comprehensive record of environmental releases and extracted resources within a geographic area over

a year) is sourced from the OpenLCA software, and the regularization outcomes are expressed utilizing a unified temporal metric: year.

(iv) Life cycle interpretation: This study compared the environmental effects of various 3DCP mix designs and determined the most noteworthy impact indicator in the concrete generation process.

3. Result and discussion

3.1. Assessment of macroscopic properties

The extruded filament was 28 mm in width, and 380 mm in length, and the maximum height of the cementitious mixture reached 400 mm as shown in Fig. 5. With a nozzle height of 410 mm, $\triangle h = 2.44\ \% < 6\ \%$, the number of printable layers significantly exceeds 30, and the structure remains stable without collapse. This indicates the material exhibits favorable buildability, characterized by appropriate plastic viscosity and static/dynamic yield stress, ensuring reliable stacking during the deposition process [36].

Fig. 6 describes the mechanical strengths of both 3D printing and cast groups containing diverse RCBP percentages at 28d. As demonstrated in Fig. 6 (a), on the X axis, the 3D printed mixture achieved its peak value of 65.57 MPa at 25-wt% RCBP substitution ratio, while registering a minimum value of 45.28 MPa at 100 % RCBP addition. In the Z direction, it attained a maximal strength of 31.33 MPa at 25-wt% RCBP replacement ratio and acquired a minimal strength of 20.31 MPa when no RCBP was incorporated. Conversely, the compressive resistance in Y orientation was roughly maintained at 50 MPa except for the 50-wt% RCBP addition group, plummeting to 35.62 MPa. Basically, the compressive results of 3DCP in X and Z directions initially increased up to a threshold of 25-wt% RCBP incorporation and subsequently declined, while Y orientation is considered the sole exception. The reduction in strength can be ascribed to the elevated RCBP content, which hinders the hydration products from generating and compromises the cohesiveness of cementitious materials. Besides, the 28d compressive strength complies with the approximate regularity: $F_z < F_y < F_x <$ mould cast.

The flexural experimental results are presented in Fig. 6 (b) and experimental data has no certain regularity with the increased RCBP. However, it is noteworthy that, compared to the flexural strengths in the x and z directions, the strength in the y direction reflects a distinct advantage. In the y direction, the flexural strength manifested values of 12.49 MPa, 12.66 MPa, 9.07 MPa, 11.30 MPa, and 8.30 MPa with RCBP additions at 0-wt%, 25-wt%, 50-wt%, 75-wt%, and 100-wt%, respectively. These values exhibited only a marginal reduction of 8.77 %, 1.17 %, 11.60 %, 6.15 %, and 10.75 % compared to the reference group. In addition, a 25-wt% RCBP replacement ratio was confirmed to generate the optimal 3D printing mixture, which holds the highest flexural strengths in the x and y directions at 8.93 MPa and 12.66 MPa, respectively, and superior performance in the z direction at 7.73 MPa. The y-axis strength manifested a notable supremacy because of the tensile force at the mid-span of the prismatic specimen remains parallel to the printed stripes. Simultaneously, the incorporated PP fiber in an organized alignment massively augments the anisotropic properties and remarkably makes contributions to deformation control and crack inhibition.

The cast group results generally witness a downward trend following the elevated RCBP according to Fig. 6. This observation is consistent with the findings of a review investigation conducted by Tang et al. [42] on the utilization of recycled concrete powder (RCP) or recycled brick powder (RBP) in novel concrete formulations. Conversely, the 3D-printed group experienced an abrupt boost in strength at 25-wt% RCBP admixture ratio, which exerts an effect similar to drainage consolidation theory [43]. Specifically, the 3D printing technology consolidates the heterogeneous area in saturated cement, reduces the air volume fraction, diminishes the inter-particle distance, accelerates the hydration rates, and eventually acquires a magnified outcome, compensating for drawbacks introduced by RCBP.

In conclusion, the mechanical characteristics of 3D printed concrete present remarkable improvement with a 25-wt% RCBP concentration. Nonetheless, the primary trend observed was a decrease in strength with increasing RCBP content. This phenomenon might be mitigated by refining the fineness of RCBP and reducing its particle size [44,45].

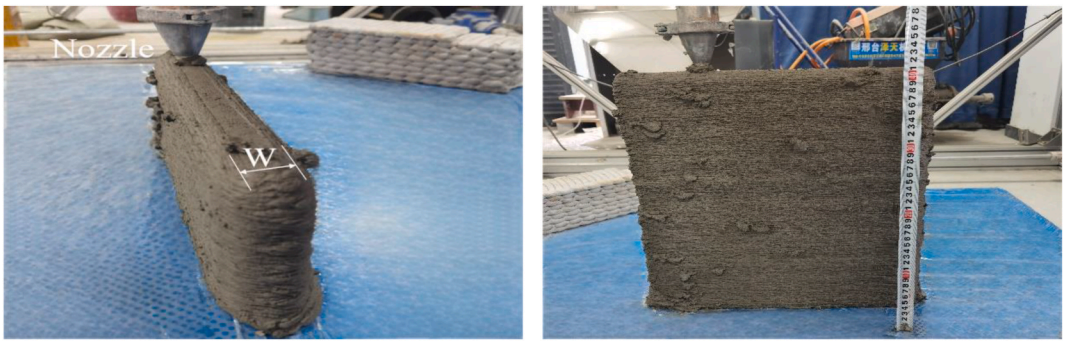

Fig. 5. Buildability test of RCBP-involved concrete.

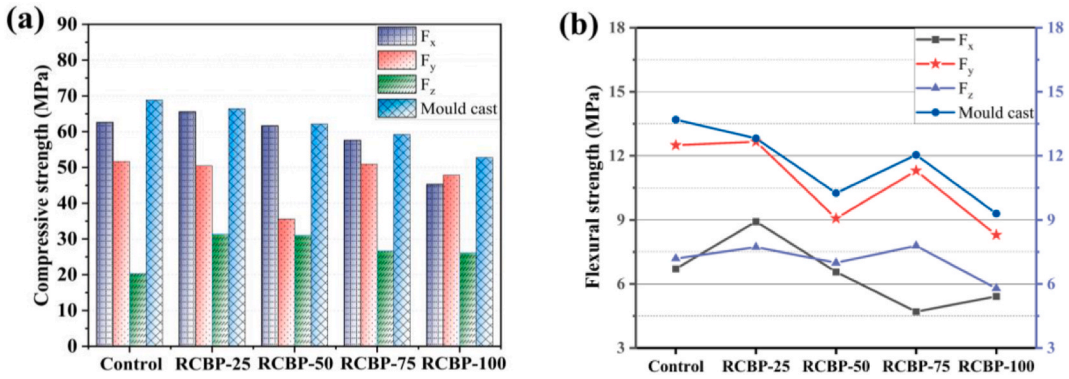

Fig. 6. Compressive strengths (a) and flexural strengths (b) of 3DCP and mould cast samples with varying RCBP content at 28 days of curing age.

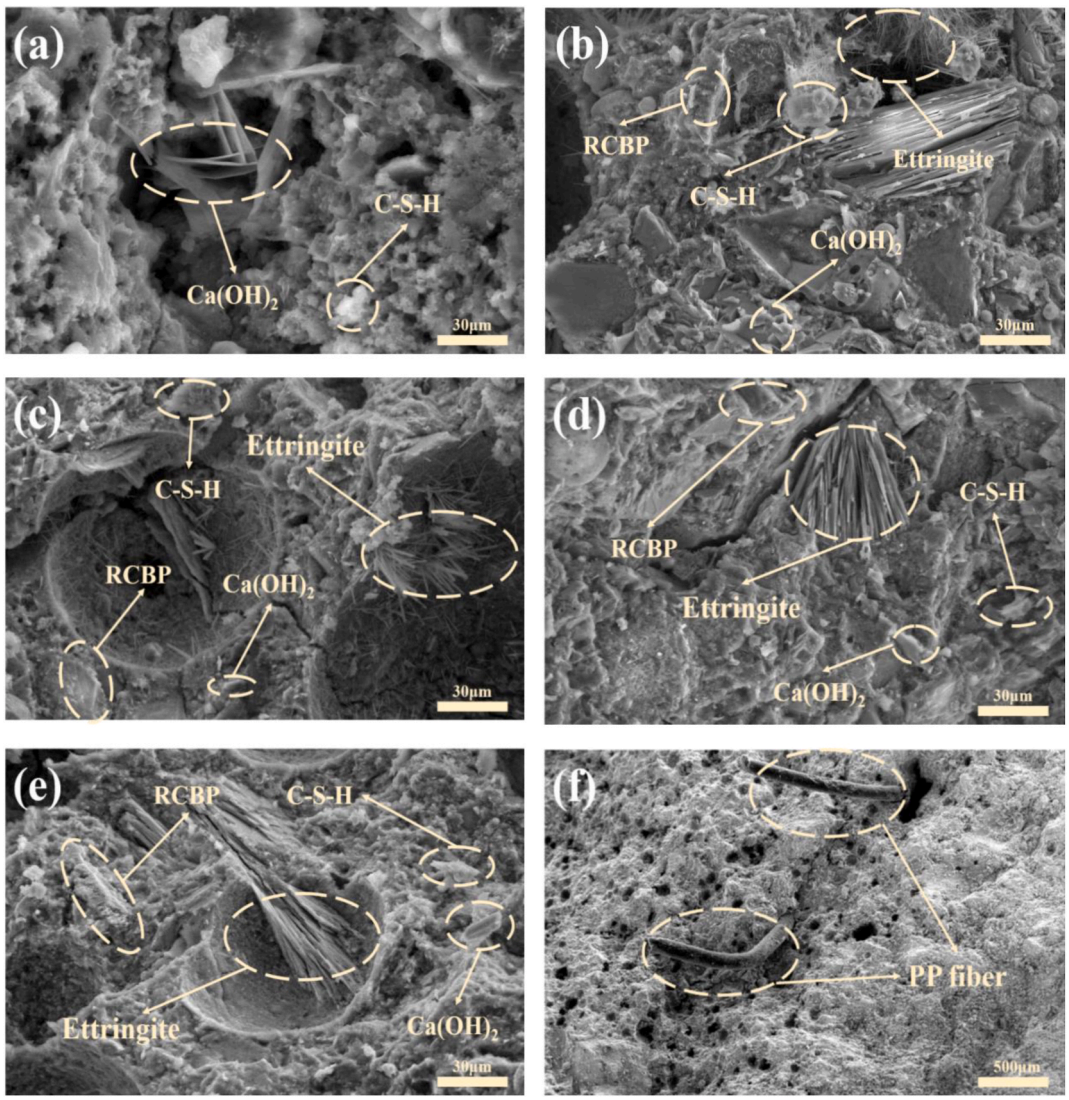

Fig. 7. SEM results of 3DCP with (a) 0-wt% RCBP, (b) 25-wt% RCBP, (c) 50-wt% RCBP, (d) 75-wt% RCBP, (e) 100-wt% RCBP, and (f) the distribution of PP fiber.

3.2. Microstructure characterization analysis utilizing SEM

3D-printed RCBP concrete microstructure morphology is depicted in Fig. 7. Various hydration products including ettringite, Ca $(OH)_2$, and C-S-H gel aggregate around the RCBP particles, as observed in Fig. 7(a)–(e). Meanwhile, oriented PP fibers remain vertical to crack direction, as demonstrated in Fig. 7 (f). Consequently, these fibers continuously suffer tensile stress and supply pullout resistance until concrete fractures into two fragmented pieces, which efficiently contributes to realizing an outstanding and anisotropic flexural performance [33,46]. Numerous studies have indicated that RCBP generally consists of components such as silica dioxide, aluminum oxide, and ferric oxide [47–49]. The two preceding comprise up to 60 % of the total RCBP content thereby creating favorable conditions for the ettringite formation. As shown in Fig. 7(b)–(e), with increasing RCBP content, the predominant morphology of ettringite gradually transitions from interwoven acicular to aggregated tabular. A 25-wt% RCBP dosage is considered optimal, attributed to the possibility that acicular ettringite may develop interwoven fiber structures within the concrete, akin to the steel reinforcement role, subsequently enhancing its flexural strength and ductility. Furthermore, acicular ettringite and fine RCBP particles effectively occlude micro-pores and cracks. Additionally, ettringite is considered an expansive cementitious material, while RCBP with a low thermal expansion coefficient mitigates the dilatation stress, contributing to preventing crack formation and consolidating compactness. Nevertheless, acicular ettringite gradually disappeared as RCBP content increased, which is mainly caused by secondary hydration reactions between more active oxides in RCBP and Ca $(OH)_2$, engendering acicular ettringite encapsulated into a dense matrix [50], transforming it into tabular or laminar ettringite. This facilitates enhanced overall bonding among different phases while still encountering obstacles in offsetting the negative influences stemming from excessive particle aggregation and insufficient hydration reactions arising from the increased RCBP content.

Eventually, fineness improvement and superior particle size distribution present exceptional potential to enlarge the specific surface area of hydration reactions, and elevate its pozzolanic activity [51,52]. Specifically, it promotes the further reaction of abundant amorphous and glass phases in RCBP with cement and $Ca(OH)_2$ to generate more hydration products and ultimately augment macro-level performance.

3.3. Porosity and pore structure exploration employing the X-CT method

0-wt%, 50-wt%, and 100-wt% RCBP are selected to display the pore structure (as shown in Fig. 8) and to conduct a mechanistic analysis. The overall porosity of the concrete decreased from 0.82 %, 0.061 %–0.045 % as the RCBP concentration escalated from 0-wt %, 50-wt% to 100-wt%, indicating that a higher RCBP substitution rate yields conducive to achieving a compact structure. This reduction is attributed to RCBP with cementitious properties occupying the cross-interfacial, intra-layer, and inter-layer voids, thereby enhancing the material's density. The substitution rate inferior to 25-wt% RCBP remarkably promotes the hydration reaction, expands the effective bonding area between aggregate particles, and optimizes the pore structure, thus reducing the porosity while enhancing the mechanical properties. However, a replacement level surpassing 25-wt% triggers an excessive RCBP accumulation, and reduces the effective contact area between aggregate particles, weakening the concrete's skeletal structure. Under this circumstance, additional microstructural issues (i.e. poor bonding between aggregate and cementitious materials, internal cracks, etc.) dominate the material properties, leading to a decrease in macroscopic mechanical strength. Consequently, high fineness and moderate RCBP substitution rate are massively recommended in that they boast merits in effectively improving the pore structure while simultaneously enhancing its mechanical properties.

Both porosity and pore geometry exert a crucial impact on macroscopic strength performance. According to the tridimensional representation of the pore distribution (as shown in Fig. 9), RCBP 3DCP demonstrates oblate spheroidal pores with the uniaxial distribution as the primary pore characteristic. Although RCBP penetrates the weak interlayer surfaces, bridges adjacent printed layers,

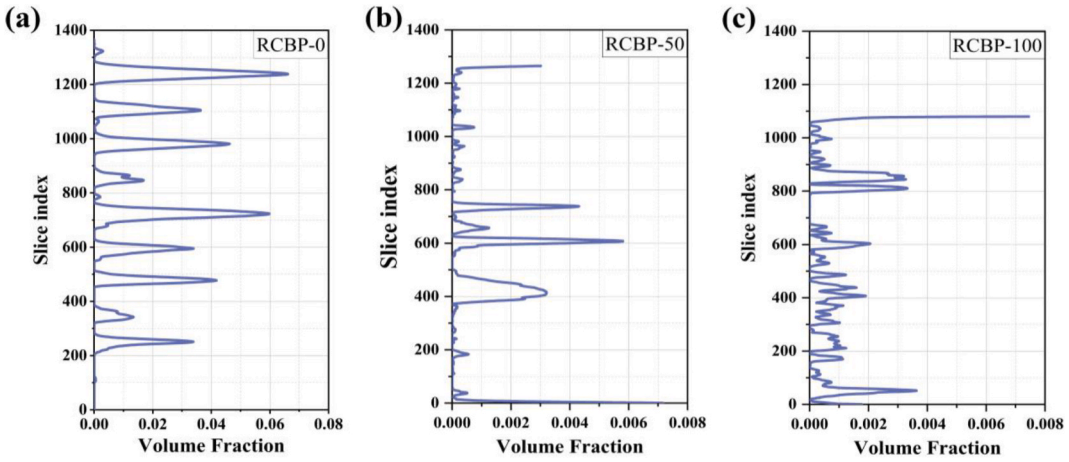

Fig. 8. Volume fraction for (a) 0-wt%, (b) 50-wt%, and (c) 100-wt% RCBP mixture.

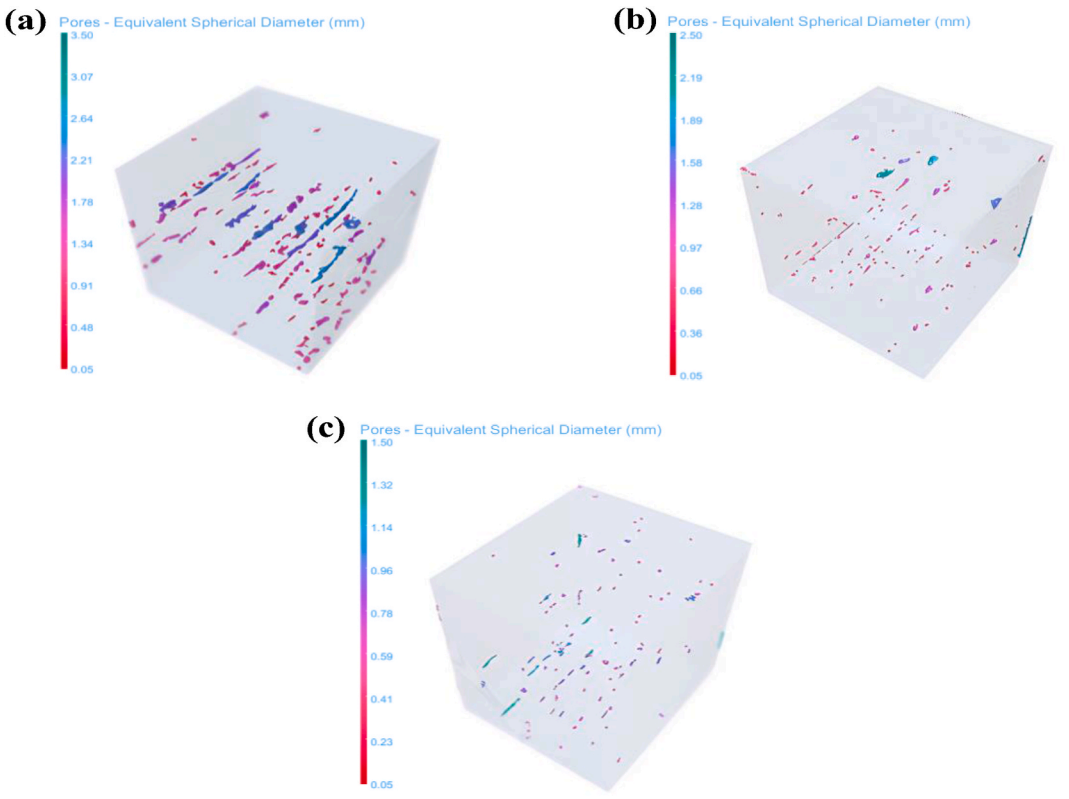

Fig. 9. Pore distribution for (a) 0-wt%, (b) 50-wt%, and (c) 100-wt% RCBP mixture.

and enhances the mechanical interlocking capabilities between layers during the 3D printing process, it also provides an opportunity for developing elongated pores in the interfacial void regions between adjacent layers [53]. The extremities of the oblate spheroidal pores are prone to local stress concentration under load, resulting in continuous expansion and crack within these directionally distributed pores. Therefore, this area is regarded as the weakest point in terms of the concrete's load-bearing performance and a primary reason for causing mechanical strength reduction and contributing to anisotropic differences. Specifically, the oblate spheroidal pores keep parallel with the loading direction along the x-axis and perpendicular to the loading directions along the y and z-axes in compressive strength tests. Consequently, the pores yielded more susceptible to stress concentration when loaded along the y and z-direction, which is perceived as the intrinsic reason why the compressive properties alongside the x-axis are superior to that along the y and z-axes. Additionally, the interlayer bonding area occupies a larger area than the intralayer bonding area, leading to interlayer failure under y-direction loading and intralayer failure under z-direction loading, thus lower loads are required to cause failure when loaded along the z-axis. The specimens exhibit maximum bending moments at the mid-span in bending tests, whose stress concentrations are likely to occur at the ends of the pore-long axes. As a result, the flexural strength under x-direction loading yields generally weaker compared to that under y and z-direction loading.

3.4. Environmental impact of the RCBP 3DCP

The cumulative impact proportions of each component in the concrete mixture are illustrated in Fig. 10. Cement reflects a dominant influence on entire ingredients on account of the considerable SO_x, NO_x, and CO_x released during the cement production process. Notably, four impact indices for antimony tailings and ceramic powder are negative signifies that these materials yield a favorable environmental impact, specifically RCBP impact value decreases from 0 % to −39.19 % as the addition increases from 0-wt% to 100-wt %. The normalization outcomes in a unified temporal metric (year) of four environmental influence indexes for 1 m^3 concrete from the OpenLCA software are demonstrated in Fig. 11.

As illustrated in Fig. 12, the concrete production process with various mix designs exerts noticeable influences on global warming potential (GWP), acidification potential (AP), and abiotic depletion (ADP), with negligible effects on stratospheric ozone depletion (ODP). Among these indicators, concrete production notably exacerbates global warming issues while minimally affecting ODP. With the RCBP content increasing from 0-wt% to 100-wt%, there is a gradual reduction observed across all indicators, respectively decreasing by 0.62 %, 6.59 %, 24.86 %, and 0.49 % for ADP, AP, GWP, and ODP, exemplifying its substantial advantages in bolstering the concrete production sustainability and alleviating environmental burdens:

ADP: The coarse sand extraction consumes substantial non-renewable resources such as river and quarry sands. Utilizing RCBP

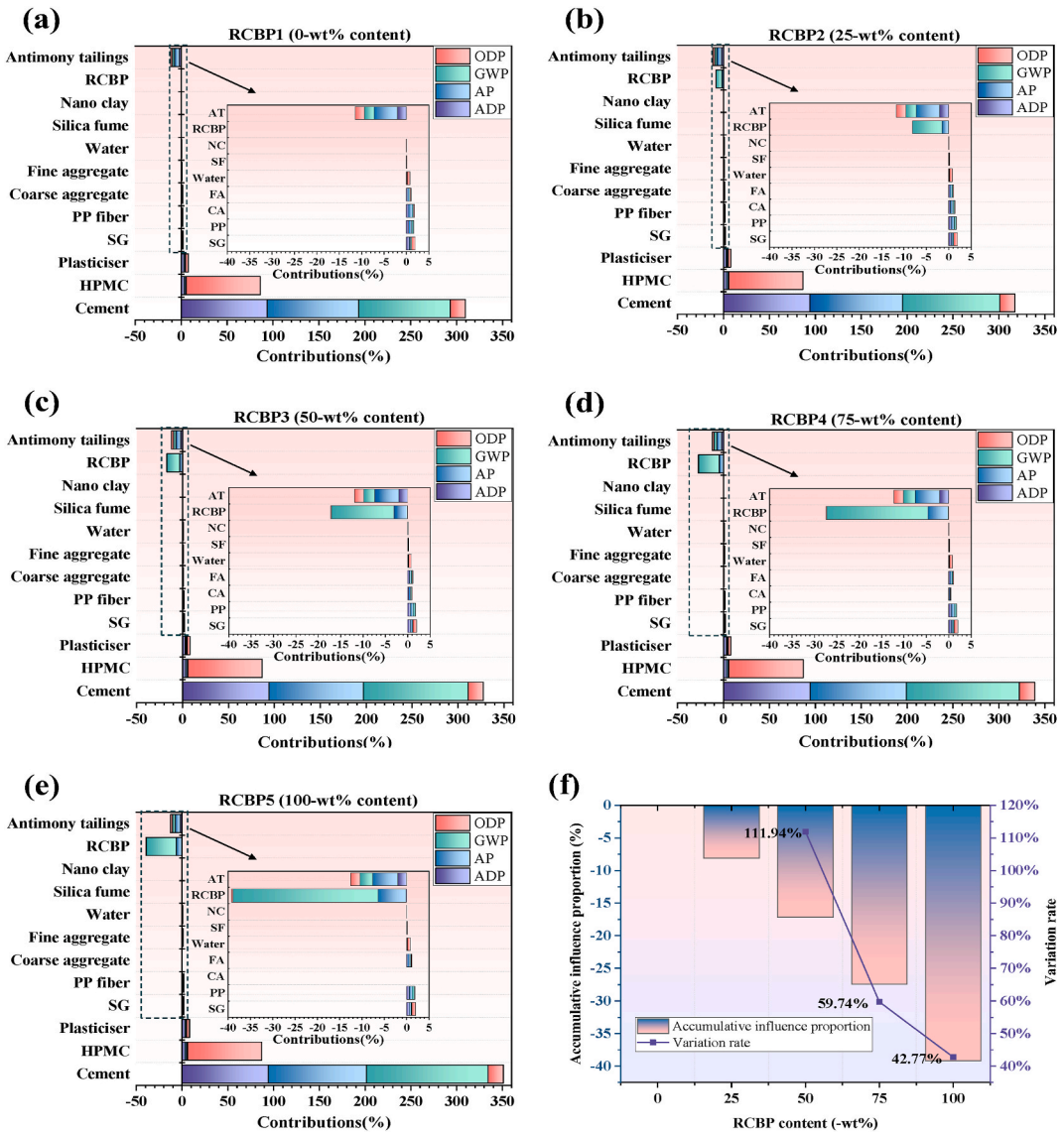

Fig. 10. The accumulative influence proportions of each constituent in the concrete mixture (a) with 0-wt% RCBP, (b) with 25-wt% RCBP, (c) with 50-wt% RCBP, (d) with 75-wt% RCBP, (e) with 100-wt% RCBP, (f) with various RCBP content.

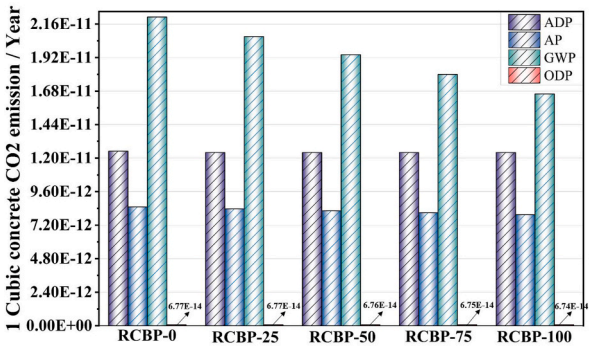

Fig. 11. Environmental impacts for 5 varieties of RCBP 3DCP mix design.

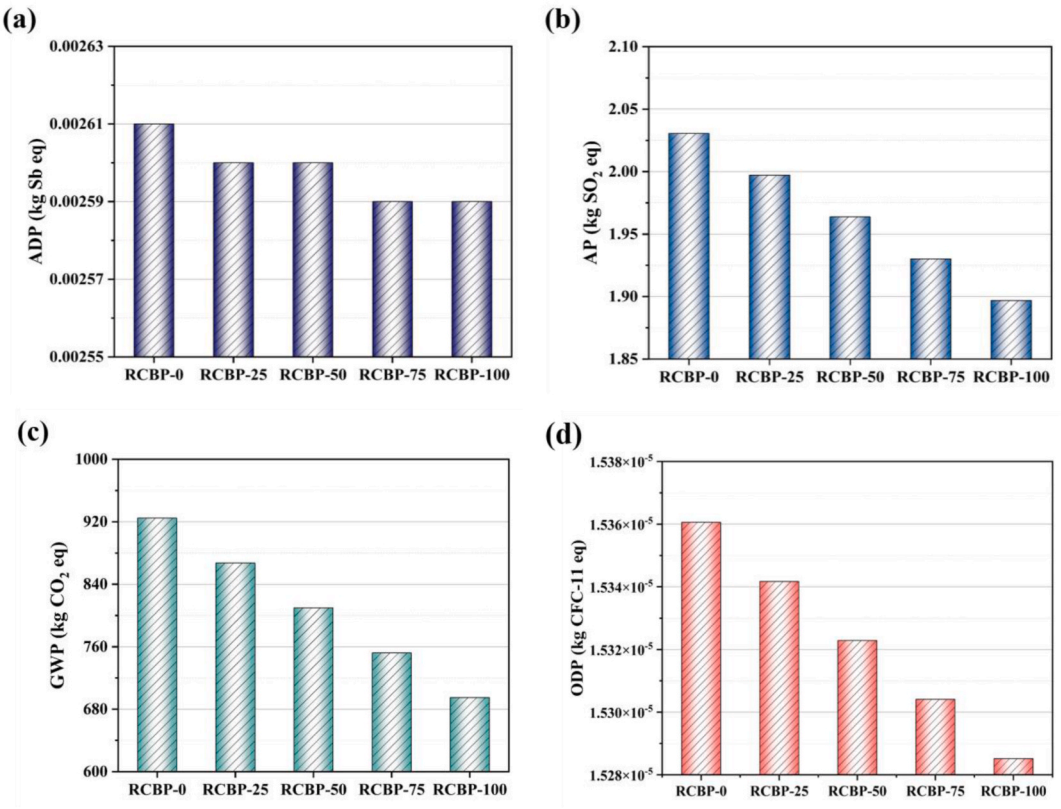

Fig. 12. The concrete numerical variations in four indicators (a) abiotic depletion, (b) acidification potential, (c) global warming potential, (d) stratospheric ozone depletion.

reduces dependency on these resources. Furthermore, 3D printing minimizes material waste and precisely controls material usage, thereby lowering ADP.

AP: Components in RCBP and the hydration products neutralize acidic substances decreased AP generated during hydration, particularly from ceramic powders. Mining and processing coarse sand often involve combustion, releasing oxides and acidic gases that contribute to AP. However, RCBP usage declines these processes, thereby diminishing AP indicators.

GWP: RCBP contains calcium oxide (CaO), which reacts with atmospheric CO_2 to form calcium carbonate ($CaCO_3$). This reaction effectively sequesters CO_2 in a solid form, reducing CO_2 concentration in the atmosphere and subsequently lowering greenhouse gas emissions. Moreover, $CaCO_3$ exists stably over long periods and does not release CO_2 back into the atmosphere so the long-term sequestration of CO_2 significantly contributes to the reduction in GWP. Additionally, RCBP applicated in durable concrete indirectly mitigates carbon emissions associated with the extraction, processing, and raw materials transportation, ultimately, these factors collectively minimize GWP.

ODP: The RCBP production and utilization are irrelevant to substances that deplete ozone, thus curtailing the impact on ODP indicators.

Consequently, on the condition that the mechanical strength is maintained, it is imperative to maximize RCBP as a substitute for coarse sand to mitigate the environmental influence of the 3DCP production process. Eventually, a 25 % RCBP mix ratio is determined as an optimal incorporation based on the comprehensive analysis of the aforementioned macroscopic mechanical test results.

4. Conclusion

In this study, fresh performance, hardened properties, microstructure, and environmental influence assessment were conducted to validate the viability of the combined RCBP and 3D-printed concrete. Anchored in the above experiment results, the main conclusion can be drawn:

(1) 3D-printed concrete employing RCBP as a replacement for traditional fine aggregates massively optimizes its rheological properties, additionally, a stacking height of 400 mm significantly reflects exceptional buildability in standability test.
(2) 3D-printed mixture equipped with 25-wt% RCBP addition was affirmed to be an optimal experimental group, whose compression and flexural strengths respectively achieved 65.57 MPa and 12.66 MPa. Nevertheless, an RCBP concentration exceeding 25-wt% impaired the strength enhancement on account of the excessive particle agglomeration. Simultaneously, the

macroscopic demonstrates prominent anisotropy in physical performance, compressive properties evinced a decisive advantage in the x-direction, while flexural performance manifests a secured dominant position in the y-axis.

(3) SEM test determined the internal mechanism that 25-wt% RCBP addition was an optimal designed mix for the following reasons. Ettringite, $Ca(OH)_2$, and C-S-H gel closely aggregate around RCBP on account of its nucleation effect significantly contributing to the hydration reaction. Meanwhile, PP fibers and acicular ettringite functioned similarly to reinforcing steel sustained tensile stress in the cracking direction. The increased ettringite was primarily attributed to the elevated RCBP proportion, with its morphology gradually transitioning from acicular to lamellar. Both ettringite morphologies are capable of filling the micropores and fissures within the concrete, supplying reinforcement against pull-out. Nonetheless, the particle accumulation and insufficient hydration reactions resulting from high RCBP concentrations adversely affect the strength development.

(4) CT experiments illustrate that the increasing RCBP replacement rate from 0-wt% to 100-wt% reduces the concrete porosity from 0.8 % to 0.045 %, indicating that RCBP and its hydrates effectively fill pores and ameliorate density. The RCBP replacement rate below 25-wt% promotes the hydration reaction, improves the pore structure, and amplifies mechanical properties. Nevertheless, excessive RCBP weakens the skeletal structure and reduces mechanical strength when the replacement rate surpasses 25-wt%. Additionally, three-dimensional pore structure images reveal that the pores are mainly oblate spheroids. RCBP possessed the capability to consolidate interlayer bonding in 3D printing, but elongated pores tend to form in interfacial areas, where stress concentration at the pore ends under load can result in negative mechanical performance. Moreover, the distribution characteristics of the three-dimensional pore structure clearly exhibit the anisotropy of the macroscopic mechanical strength and the reasons for the differences.

(5) RCBP incorporated in 3D printing concrete exhibits positive and eco-friendly environmental impact indicated by GWP, AP, ODP, and ADP. Four indicator values for RCBP maintain negative and realize outstanding −39.19 % at 100-wt% concentration. Specifically, RCBP exerts a massive influence on GWP because of the 24.86 % reduction as its inclusion arises from 0-wt% to 100-wt%, which is significantly attributed to the carbon sequestration capability of RCBP.

In conclusion, RCBP with high fineness and moderate content will fully exploit the merits of 3D printing technology, achieving a superior microstructure and enhanced overall strength, while also potentially contributing more significantly to environmental sustainability.

CRediT authorship contribution statement

Bo Huang: Supervision, Methodology, Conceptualization. **Yutian Ge:** Writing – review & editing, Writing – original draft. **Xiangyu Wang:** Data curation. **Yufei Wang:** Formal analysis. **Jianqun Wang:** Investigation. **Chengwei Song:** Project administration. **Jun Zhu:** Resources. **Chiemela Victor Amaechi:** Software. **Junbo Sun:** Visualization, Validation.

Declaration of competing interest

The authors declare that they have no known competing financial interests or personal relationships that could have appeared to influence the work reported in this paper.

Acknowledgments

The support from the Natural Science Foundation of Hunan Province (2024JJ5159, 2024JJ6217) is greatly appreciated.

Data availability

Data will be made available on request.

References

[1] The world bank, Solid waste management. https://www.worldbank.org/en/topic/urbandevelopment/brief/solid-waste-management, 2022. (Accessed 2 August 2024).
[2] A. Mohajerani, L. Burnett, J.V. Smith, S. Markovski, G. Rodwell, M.T. Rahman, et al., Recycling waste rubber tyres in construction materials and associated environmental considerations: a review, Resour. Conserv. Recycl. 155 (2020) 104679.
[3] B. Huang, Y. Chi, T. Almotlaq, J. Wang, M. Saafi, J. Ye, et al., Influence of sugar beetroot microsheets on the hydration kinetics of cementitious composites: electrochemical characterization, Cement Concr. Compos. 144 (2023) 105314.
[4] B. Huang, Y. Chi, J. Wang, G. Wang, J. Ye, E. Whale, et al., Mechanical and fracture properties of sugar beetroot-based nanosheets (SNS) doped cementitious composites, Construct. Build. Mater. 409 (2023) 133926.
[5] T. Almotlaq, B. Huang, M. Saafi, J. Ye, Enhancing the self-sensing and energy storage capabilities of cementitious composites through marine sand doping, Construct. Build. Mater. 428 (2024) 136218.
[6] W. Ferdous, A. Manalo, R. Siddique, P. Mendis, Y. Zhuge, H.S. Wong, et al., Recycling of landfill wastes (tyres, plastics and glass) in construction–A review on global waste generation, performance, application and future opportunities, Resour. Conserv. Recycl. 173 (2021) 105745.
[7] A. Bakchan, K.M. Faust, Construction waste generation estimates of institutional building projects: leveraging waste hauling tickets, Waste Manag. 87 (2019) 301–312.

[8] K. Pasupathy, S. Ramakrishnan, J. Sanjayan, 3D concrete printing of eco-friendly geopolymer containing brick waste, Cement Concr. Compos. 138 (2023) 104943.
[9] B. Wang, L. Yan, Q. Fu, B. Kasal, A comprehensive review on recycled aggregate and recycled aggregate concrete, Resour. Conserv. Recycl. 171 (2021) 105565.
[10] S. Ray, M. Haque, M.N. Sakib, A.F. Mita, M.M. Rahman, B.B. Tanmoy, Use of ceramic wastes as aggregates in concrete production: a review, J. Build. Eng. 43 (2021) 102567.
[11] Q. Tang, Z. Ma, H. Wu, W. Wang, The utilization of eco-friendly recycled powder from concrete and brick waste in new concrete: a critical review, Cement Concr. Compos. 114 (2020) 103807.
[12] J. Dang, J. Zhao, S. Dai Pang, S. Zhao, Durability and microstructural properties of concrete with recycled brick as fine aggregates, Construct. Build. Mater. 262 (2020) 120032.
[13] P. Sahoo, A. Dwivedi, S.M. Tuppad, S. Gupta, Sequestration and utilization of carbon dioxide to improve engineering properties of cement-based construction materials with recycled brick powder: a pathway for cleaner construction, Construct. Build. Mater. 395 (2023) 132268.
[14] M. Shrivastava, H. Tsegaye, S. Kumar, K.V. Harish, Assessment of hydration behaviour of Portland Cement-Based materials containing brick powders as partial replacement for fine aggregates, Mater. Today: Proc. 65 (2022) 1095–1104.
[15] D. Kovaleva, M. Nistler, A. Verl, L. Blandini, W. Sobek, Zero-waste production of lightweight concrete structures with water-soluble sand formwork. Third RILEM International Conference on Concrete and Digital Fabrication, Springer, 2022, pp. 3–8.
[16] Y. Zhang, Y. Zhang, W. She, L. Yang, G. Liu, Y.J.C. Yang, Rheological and harden properties of the high-thixotropy 3D printing concrete, Construct. Build. Mater. 201 (2019) 278–285.
[17] M.A. Hossain, A. Zhumabekova, S.C. Paul, J.R. Kim, A review of 3D printing in construction and its impact on the labor market, Sustainability 12 (2020) 8492.
[18] N. Shahrubudin, T.C. Lee, R. Ramlan, An overview on 3D printing technology: technological, materials, and applications, Procedia Manuf. 35 (2019) 1286–1296.
[19] S. El-Sayegh, L. Romdhane, S. Manjikian, A critical review of 3D printing in construction: benefits, challenges, and risks, Arch. Civ. Mech. Eng. 20 (2020) 1–25.
[20] J. Sun, W. Tang, Y. Wang, X. Yao, B. Huang, M. Saafi, et al., Electromagnetic and mechanical performance of 3D printed wave-shaped copper solid superstructures, J. Mater. Res. Technol. 27 (2023) 6936–6946.
[21] C.V. Amaechi, E.F. Adefuye, I.M. Kgosiemang, B. Huang, E.C. Amaechi, Scientometric review for research patterns on additive manufacturing of lattice structures, Materials 15 (2022) 5323.
[22] J. Xiao, G. Ji, Y. Zhang, G. Ma, V. Mechtcherine, J. Pan, et al., Large-scale 3D printing concrete technology: current status and future opportunities, Cement Concr. Compos. 122 (2021) 104115.
[23] I. Muñoz, J. Alonso-Madrid, M. Menéndez-Muñiz, M. Uhart, J. Canou, C. Martin, et al., Life cycle assessment of integrated additive–subtractive concrete 3D printing, Int. J. Adv. Des. Manuf. Technol. 112 (2021) 2149–2159.
[24] A. Rahul, M.K. Mohan, G. De Schutter, K. Van Tittelboom, 3D printable concrete with natural and recycled coarse aggregates: rheological, mechanical and shrinkage behaviour, Cement Concr. Compos. 125 (2022) 104311.
[25] H. Liu, C. Liu, Y. Wu, G. Bai, C. He, R. Zhang, et al., Hardened properties of 3D printed concrete with recycled coarse aggregate, Cement Concr. Res. 159 (2022) 106868.
[26] T. Ding, J. Xiao, S. Zou, Y. Wang, Hardened properties of layered 3D printed concrete with recycled sand, Cement Concr. Compos. 113 (2020) 103724.
[27] G. Ma, Z. Li, L. Wang, Printable properties of cementitious material containing copper tailings for extrusion based 3D printing, Construct. Build. Mater. 162 (2018) 613–627.
[28] J. Liu, S. Li, C. Gunasekara, K. Fox, P. Tran, 3D-printed concrete with recycled glass: effect of glass gradation on flexural strength and microstructure, Construct. Build. Mater. 314 (2022) 125561.
[29] A. Singh, Y. Wang, Y. Zhou, J. Sun, X. Xu, Y. Li, et al., Utilization of antimony tailings in fiber-reinforced 3D printed concrete: a sustainable approach for construction materials, Construct. Build. Mater. 408 (2023) 133689.
[30] C. Yang, X. Xu, Z. Lei, J. Sun, Y. Wang, G. Luo, et al., Enhancing mechanical properties of three-dimensional concrete at elevated temperatures through recycled ceramic powder treatment methods, J. Mater. Res. Technol. 31 (2024) 434–446.
[31] J. Sun, F. Aslani, J. Lu, L. Wang, Y. Huang, G. Ma, Fibre-reinforced lightweight engineered cementitious composites for 3D concrete printing, Ceram. Int. 47 (2021) 27107–27121.
[32] V. Letelier, J.M. Ortega, P. Muñoz, E. Tarela, G. Moriconi, Influence of waste brick powder in the mechanical properties of recycled aggregate concrete, Sustainability 10 (2018) 1037.
[33] Q. Liu, B. Li, J. Xiao, A. Singh, Utilization potential of aerated concrete block powder and clay brick powder from C&D waste, Construct. Build. Mater. 238 (2020) 117721.
[34] V. Letelier, E. Tarela, G. Moriconi, Mechanical properties of concretes with recycled aggregates and waste brick powder as cement replacement, Procedia Eng. 171 (2017) 627–632.
[35] J. Xiao, Z. Ma, T. Sui, A. Akbarnezhad, Z. Duan, Mechanical properties of concrete mixed with recycled powder produced from construction and demolition waste, J. Clean. Prod. 188 (2018) 720–731.
[36] F. Li, Y. Lu, W. Li, X. Xu, Study on printability of mortar for 3D printing, Bull. Chin. Ceram. Soc. 43 (2024) 1615–1622.
[37] GB/T 50081-2002, Standard for Test Method of Mechanical Properties on Ordinary Concrete, State Bureau of Quality and Technical Supervision, 2002.
[38] GB/T 17671-1999, Method of Testing Cements - Determination of Strength, 1999. Beijing, China.
[39] Technical Committee ISO/TC 207 EM, Environmental Management-Life Cycle Assessment-Principles and Framework, International Organization for Standardization, 2006.
[40] Sustainability of Construction Works—Environmental Product Declarations—Core Rules for the Product Category of Construction Products. Brussels BECfS, 2012.
[41] V. Prado, B.A. Wender, T.P. Seager, Interpretation of comparative LCAs: external normalization and a method of mutual differences, Int. J. Life Cycle Assess. 22 (2017) 2018–2029.
[42] Q. Tang, Z. Ma, H. Wu, W. Wang, The utilization of eco-friendly recycled powder from concrete and brick waste in new concrete: a critical review, Cement Concr. Compos. 114 (2020) 103807.
[43] M. Abedini, C. Zhang, Dynamic vulnerability assessment and damage prediction of RC columns subjected to severe impulsive loading, Struct. Eng. Mech. 77 (2021) 441–461. An Int'l Journal.
[44] J.M. Ortega, V. Letelier, C. Solas, G. Moriconi, M.Á. Climent, I. Sánchez, Long-term effects of waste brick powder addition in the microstructure and service properties of mortars, Construct. Build. Mater. 182 (2018) 691–702.
[45] L. Zheng, Z. Ge, Z. Yao, Z. Gao, Mechanical properties of mortar with recycled clay-brick-powder, ICCTP (2011) 3379–3388. Towards Sustainable Transportation Systems2011.
[46] R. Hay, K. Celik, Hydration, carbonation, strength development and corrosion resistance of reactive MgO cement-based composites, Cement Concr. Res. 128 (2020) 105941.
[47] L. Reig, M.M. Tashima, M. Borrachero, J. Monzó, C. Cheeseman, J. Payá, Properties and microstructure of alkali-activated red clay brick waste, Construct. Build. Mater. 43 (2013) 98–106.
[48] R.A. Robayo, A. Mulford, J. Munera, R.M. De Gutiérrez, Alternative cements based on alkali-activated red clay brick waste, Construct. Build. Mater. 128 (2016) 163–169.
[49] J. Shao, J. Gao, Y. Zhao, X. Chen, Study on the pozzolanic reaction of clay brick powder in blended cement pastes, Construct. Build. Mater. 213 (2019) 209–215.
[50] L. Zhao, Study on Basic Properties and Application of Recycled Fine Powder from Construction Waste, Beijing University of Civil Engineering, 2019.

[51] E. Navrátilová, P.J.C. Rovnaníková, Pozzolanic properties of brick powders and their effect on the properties of modified lime mortars, Construct. Build. Mater. 120 (2016) 530–539.
[52] D. Yang, M. Liu, Z. Ma, Properties of the foam concrete containing waste brick powder derived from construction and demolition waste, J. Build. Eng. 32 (2020) 101509.
[53] H. Liu, C. Liu, Y. Wu, G. Bai, C. He, R. Zhang, et al., Hardened properties of 3D printed concrete with recycled coarse aggregate, Cement Concr. Res. 159 (2022) 106868.